Relationship Between Crystallization Behavior, Microstructure, and Mechanical Properties in a Palm Oil-Based Shortening

J.W. Litwinenko[a], A.M. Rojas[b], L.N. Gerschenson[b,c], and A.G. Marangoni[a,*]

[a]Department of Food Science, University of Guelph, Guelph, Ontario, Canada N1G 2W1, [b]Departamento de Industrias, Facultad de Ciencias Exactas y Naturales, Universidad de Buenos Aires, 1428 Buenos Aires, Argentina, and [c]National Research Council, Argentina (CONICET)

ABSTRACT: In this study, the effects of cooling rate, degree of supercooling, and storage time on the microstructure and rheological properties of a vegetable shortening composed of soybean and palm oils were examined. The solid fat content vs. temperature profile displayed two distinct regions: from 5 to 25°C, and from 25°C to the end of melt at 45–50°C. A peak melting temperature of 42.7°C was determined by DSC. Discontinuity in the crystallization induction time (determined by pulsed NMR) vs. temperature plot at 27°C also suggested the existence of two separate groups of crystallizing material. Isothermal crystallization kinetics were characterized using the Avrami and Fisher–Turnbull models. In using DSC and powder X-ray diffraction, the α polymorph formed upon fast cooling (>5°C/min), and the β′ form predominated at lower cooling rates (<1°C/min). An α to β′ transition took place upon storage. Fractal dimensions (D_f) obtained by microscopy and image analysis showed no dependence on the degree of supercooling since D_f remained constant (~1.89) at crystallization temperatures of 5, 22, and 27°C. Crystallization at 22°C at 1°C/min and 15°C/min yielded D_f values of 1.98 and 1.93, respectively. Differences in microstructure were observed, and changes in particle properties increased the parameter λ at higher degrees of supercooling.

Paper no. J10102 in *JAOCS 79,* 647–654 (July 2002).

KEY WORDS: Crystallization, fractal dimension, microstructure, palm oil, polymorphism, rheology, shortening.

Hydrogenation of unsaturated FA in edible oils allows for the conversion of liquid oils into semisolid fats. These fats are characterized by altered melting and textural characteristics and by a higher oxidative stability. Modified plastic vegetable fats are often the key ingredients in margarines and specialty tailored fats like shortening (1).

Shortenings are commonly used in dough formulations where the fats need to be mixed with other ingredients at room temperature and possess a high level of stability at elevated baking temperatures. Therefore, a smooth material that is spreadable at room temperature and has a specific melting profile, solid fat content (SFC), and polymorphic behavior is desired.

It is well known that the solid-like behavior of plastic fats is due to the presence of a fat crystal network (2–5). The influence of microstructure on the macroscopic rheological properties of shortening is therefore the focus of this study. The nature of this crystal network, including its spatial distribution, and the number, size, and shape of its constituent microstructural elements can be dramatically altered by changes in crystallization conditions. Effects of cooling rate, the degree of supercooling, and storage time on crystallization and melting behavior and mechanical properties, including the storage modulus (G') and loss modulus (G''), were investigated. Powder X-ray diffraction (XRD) spectroscopy and DSC were also used to investigate the effects of various crystallization conditions on polymorphism in the shortening.

MATERIALS AND METHODS

Sample and chemicals. A commercially available all-vegetable oil-based shortening (Golden Crisco Doré, Procter & Gamble, Toronto, Ontario, Canada) composed mainly of partially hydrogenated soybean and palm oils was studied. Hydrogenated modified palm oil, mono- and diglycerides, and artificial flavor and color were also present in the shortening. In retail environments the product is usually displayed at room temperature (approximately 21°C). Chemicals used in the experiments were purchased from Fisher Scientific (St. Louis, MO) and Sigma Chemical (St. Louis, MO). High-purity nitrogen and helium from BOC Gases (Guelph, Ontario, Canada) were used.

Lipid composition. Compositional analysis was performed by GLC using a Shimadzu GC-8A (Tokyo, Japan) and an FID operated at 360°C as previously described (8). TAG analysis was performed on the basis of carbon number. FA composition was also determined using the same apparatus following derivatization of the samples to FAME (9). The injector port temperature was 230°C, and runs were performed by ramping from 60 to 210°C at 5°C/min.

SFC. SFC was measured by pulsed NMR (pNMR) with a Bruker PC/20 Series NMR Analyzer (Bruker, Milton, Canada). Melting profiles of the shortening were obtained by holding the samples at 80°C for 30 min to erase any crystal history. The melted fat was then placed in NMR tubes (four replicates) and submitted to the tempering treatments of the AOCS serial method Cd 16-81 (10). The SFC was determined in the range of 0–55°C at 5°C intervals following 30-min incubations at each temperature.

*To whom correspondence should be addressed.
E-mail: amarango@uoguelph.ca

Crystallization kinetics. Crystallization kinetics were investigated at the following temperatures: 5, 10, 15, 20, 22, 25, 27, 30, 32, 35, and 38°C. Four replicates of each sample were melted in NMR tubes at 80°C for 30 min to erase any crystal history and then held at 60°C for 30 min. Crystallization curves were obtained at each of the aforementioned temperatures by placing the tubes in water baths and taking SFC readings at the appropriate time intervals. The crystallization curves were fitted to the Avrami equation by least squares nonlinear regression (11). Avrami's theory describes changes in the volume of the crystal mass as a function of time during a phase change. The Avrami equation is applied to fat systems as:

$$\mathrm{SFC}(t) = \mathrm{SFC}_{\infty}\left[1 - \exp\left(-kt^{n}\right)\right] \quad [1]$$

where SFC(t) and SFC_{∞} are the SFC (%) at time t and the maximum SFC after crystallization is completed, respectively. Fitting the SFC data to this model allows for the determination of the rate constant of crystallization (k) at a particular temperature (T), and the mechanism of nucleation and crystal growth *via* the exponent (n) (12,13).

Induction time of crystallization (τ). Induction times were determined in triplicate using a cloud point analyzer (Fats and Oils Analyzer PSA-70V-HT, Phase Technology, Richmond, British Columbia, Canada). A shortening sample (150 μL), heated to 80ºC for 30 min, was pipetted into the sample chamber, which was preheated to 70ºC. The sample chamber was then rapidly cooled at a rate of 30ºC/min to crystallization temperatures of 5, 10, 15, 20, 22, 24, 25, 26, 27, 30, 32, 35, and 38°C. On the basis of scattered-light intensity measurements, the apparatus provides information on the changes in crystal mass as a function of time. Induction times (τ) of crystallization are determined by extrapolating from the linearly increasing portion of the curve to the time axis.

By using τ, the apparent free energies of nucleation (ΔG_c) were determined at each temperature. ΔG_c depends on the degree of supercooling ($\Delta T = T_m - T$), which can influence polymorphic form and microstructure. With sufficient supercooling, a melt becomes supersaturated and nucleation occurs, resulting in a lowering of the overall free energy of the system. In this study, the free energy of nucleation was calculated using the Fisher–Turnbull equation as described in previous studies (13).

DSC. The effects of cooling rate, storage, and final crystallization temperature on the crystallization and melting behavior of the shortening were evaluated by DSC. Calorimetric analysis was performed with a DuPont 2910 DSC (TA Instruments, Mississauga, Ontario, Canada). Nitrogen and helium purge gases were used to prevent condensation in the cell, and an empty pan was used as reference. Shortening samples (7–9 mg), with crystal history erased, were loaded in aluminum pans, hermetically sealed, and stored for 72 h at 5.0°C before analysis. Melting was then performed on these samples (in triplicate) by heating the pans from 5 to 60ºC at a constant temperature ramp of 5°C/min. The peak melting temperature (T_m) of 42.7ºC was used for free energy of nucleation calculations.

The influence of cooling rate and degree of supercooling on crystallization behavior was examined by cooling separate samples from 60 to 5°C and 23°C under the following constant rates: 15, 5, 1, and 0.5°C/min. To examine the effects of storage on the melting behavior, samples crystallized at these four different rates were subjected to either immediate heating to 60.0°C (at 5°C/min) or storage for 48 h at 5 and 23°C.

XRD spectroscopy. Powder XRD spectroscopy was performed using an Enraf-Nonius KappaCCD diffractometer (Nonius, Delft, The Netherlands) with an FR590 X-ray generator. Shortening samples were quench-cooled and stored at 5, 22, and 26ºC for 6 d prior to analysis. Another set of samples was quench-cooled to 28, 23, and 5ºC and examined after just 5 to 7 min of storage. Last, another sample was cooled slowly in a stepwise manner by placing it into incubators for 1 h at each of the following temperatures: 80, 60, 26, 22, and for 5 min at 5ºC prior to analysis. The *d*-spacings were calculated by comparing the spacings of the rings in these images to those of a standard ($CaSO_4 \cdot 2H_2O$). Polymorphic forms were determined from the *d*-spacings.

Rheology. Rheological measurements at small deformations were made using a CarriMed CSL^2 500 Rheometer (TA Instruments) with a 2-cm flat plate attachment. The sample platform temperature was controlled, allowing for samples to be analyzed at specific temperatures (5, 22, and 27°C). Melted samples were poured into cylindrical molds of uniform diameter (20 mm) and thickness (3.2 mm) and were crystallized and stored at 5, 22, and 27°C for 72 h. The linear viscoelastic region (LVR) for each sample was first determined by performing oscillatory stress sweeps from 0.65 to 400 Pa at a constant frequency of 1 Hz. A constant strain of 5×10^{-3}% was then chosen, and a frequency sweep (0.1–10 Hz) was performed within the LVR of all samples. Care was taken to follow the tempering procedure used for the shortening during preparation of the samples for rheology.

Spatial distribution of mass by polarized light microscopy (PLM) and image analysis. A small droplet (about 10 μL) of melted fat (80ºC for 30 min) was placed on a preheated (80ºC) glass slide, using a preheated capillary tube. A preheated glass cover slip was carefully placed over the sample to produce a film of uniform thickness. The slides were then stored for 10 min at 60°C. To investigate the effects of cooling rate, samples were crystallized at 22ºC by cooling at both 15 and 1ºC/min using a thermostatically controlled microscope stage (Linkam, Tadworth, Surrey, United Kingdom). These same samples were then stored for 48 h at 22ºC and imaged again in order to examine the effects of short-term storage. In order to examine the effects of the degree of supercooling, melted samples at 60ºC were placed directly into incubators at 27, 22, and 5ºC and stored for 72 h before imaging. When viewed by PLM (Olympus BH, Tokyo, Japan), the birefringent solid microstructural elements of the network could be directly observed, and digital images were acquired *via* a black-and-white Sony XC75 CCD camera and video capture board (Scion, Frederick, MD). The images were then inverted, thresholded, and analyzed using a particle-counting

algorithm in order to determine the fractal dimension (D_f) (5). The number of particles (N) counted within box sizes of varying length (L) were examined on a log-log plot. The slope of the linear regression corresponds to D_f. The method used to calculate D_f was altered slightly from previous experiments to improve accuracy. Boxes of decreasing size were laid over the micrographs and the number of particles counted. These counts were performed twice on each image—once including all particles touching the edge of the region of interest, and once excluding those that touch the edges. By taking the average of these two counts, a D_f that best represents the spatial distribution of mass is obtained.

Microstructural parameters. Microstructural parameters were investigated using a model that relates rheological properties to particle properties, SFC and the spatial distribution of mass of a crystal network by the following equation:

$$G' = \lambda\phi^m \quad [2]$$

where G' is the storage modulus (from rheological experiments), ϕ is the volume fraction of solids (SFC/100), $m = 1/(3 - D_f^{3d})$, and D_f^{3d} is the fractal dimension computed by image analysis translated into three dimensions. Furthermore, our group has developed a model for λ:

$$\lambda \sim \frac{A^3}{\pi a d_o^2} \quad [3]$$

where A is Hamacker's constant, a is the diameter of the particles within a floc, and d_o is the average distance between clusters (6,7). The exact mathematical expression for the λ value can vary dramatically depending on the morphology of the flocs (if the interaction occurs between spheres, blocks, or between particles with a shape intermediate between blocks and spheres). Thus, the shape of the clusters can greatly influence the value of the elastic modulus (6,7). In fat systems where λ value greatly contributes to the mechanical behavior of the system subjected to very small deformations within the linear viscoelastic region, the morphology and size of the microstructural elements also affects the mechanical strength of the network. The percentage area of black pixels (representing birefringent crystal mass) of the inverted and thresholded images was therefore computed, the number of particles counted, and the mean particle diameter determined (assuming circular geometry).

RESULTS AND DISCUSSION

Compositional analysis. FA and TAG composition of the shortening revealed information on the probable quantities of palm and soybean oils present in the mixture (Table 1). Oleic acid (18:1) and linoleic acid (18:2) combined accounted for 67.8% of the total FA present, and palmitic acid (16:0) 18.2%. Soybean oil was responsible for the contribution of α-linolenic acid (18:3), which represented about 5.1% of the total FA in the mixture. By taking into account that α-linolenic acid in pure soybean oil is usually 8% (14), it is reasonable to conclude that the shortening studied contained no less than 63% soybean oil. Relatively high homogeneity in the molecular structure of the TAG was observed since C_{50}, C_{52}, and C_{54} combined to make up 88.7% of the total. The majority of the tripalmitin (C_{48}) was contributed by the palm oil. The composition of the shortening influences its physical properties, particularly melting behavior, and hence has a profound influence on the macroscopic textural properties of the fat (15).

TABLE 1
FA and TAG Composition of Shortening Composed of Partially Hydrogenated Palm and Soybean Oil[a]

FA	Composition (wt%)	TAG (carbon number)	Composition (wt%)
12:0	0.55 ± 0.00	46	4.22 ± 0.03
14:0	1.83 ± 0.01	48	5.51 ± 0.01
16:0	18.22 ± 0.3	50	10.84 ± 0.06
17:0	0.21 ± 0.00	52	28.4 ± 0.22
17:1	0.10 ± 0.01	54	49.44 ± 0.41
18:0	4.82 ± 0.03	56	1.59 ± 0.01
18:1	42.54 ± 0.22		
18:2	25.26 ± 0.30		
18:3	5.08 ± 0.03		
22:0	1.40 ± 0.02		

[a]Determined by GLC. Data reported represent the average of two replicates and the SD ($P < 0.05$).

SFC. The melting profile obtained for the shortening by NMR (Fig. 1) showed that it had ~12% SFC at 21°C, the temperature at which this shortening is stored in retail environments. The maximum SFC observed was ~20% and occurred at temperatures between 0 and 5°C. All solids melted in the range of 45–50°C. The SFC decreased in a linear fashion as temperature increased from 5 to 20°C, followed by a small region between 20 and 30ºC with a less accentuated slope. Between 30 and 50ºC, the SFC again decreased linearly with temperature with a slope similar to the melting behavior at low temperatures. The observed changes in slope are due to contributions from the various TAG fractions present in the material.

Crystallization kinetics and free energy of nucleation. As anticipated, maximal SFC at each temperature was comparable to that arrived at in the melting profile of Figure 1, and the induction times were longer at higher temperatures (Fig. 2A). The SFC-time curves were fitted to the Avrami model, and values of Avrami exponent (n) were calculated (Fig. 2B). Values

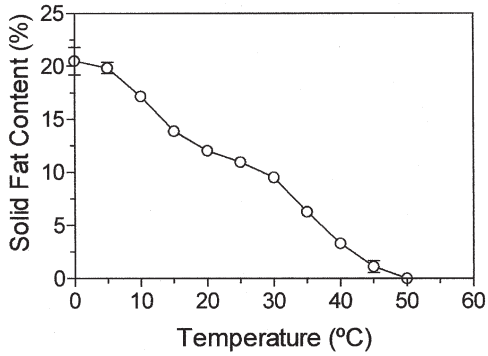

FIG. 1. Solid fat content (%) vs. temperature (°C) for the shortening. Symbols and error bars represent the mean ± SD of four replicates.

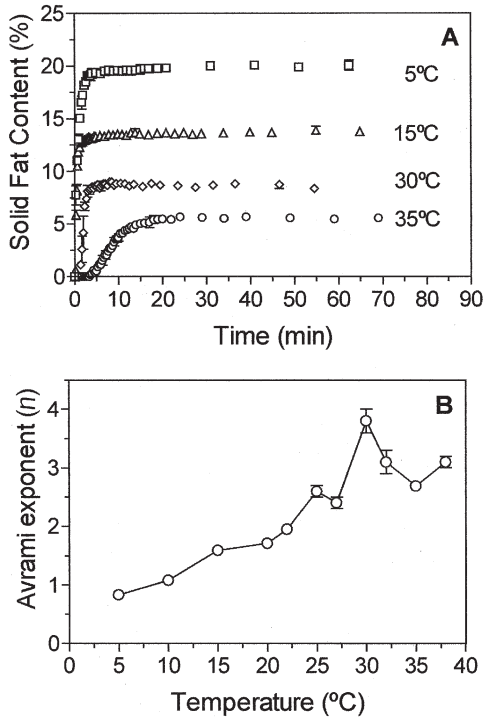

FIG. 2. (A) Solid fat content (%) vs. time (min). Solid fat content was measured by pulsed NMR at appropriate times. Symbols and error bars represent the mean ± SD of four replicates. (B) Avrami exponents *n* for the shortening as a function of crystallization temperature. They were calculated from the curves of crystallization kinetics (A).

for the Avrami exponent describe the type of crystal nucleation and growth and are represented by integer numbers between 1 and 4 in the Avrami theory of the kinetics of phase change (12,13,16). In this study, the Avrami exponent (*n*) generally increased with increasing temperature, from approximately 1 to 4. Values of 1 correspond to rod-like growth from instantaneous nuclei, whereas spherulitic growth from sporadic nuclei is expected when a value of 4 is obtained (13). These morphological characteristics were also detected by PLM (Fig. 6).

Kinetics of crystallization were also examined using a cloud point analyzer, and data were analyzed using the Fisher–Turnbull equation as previously described (13). Owing to difficulties in accurately measuring induction times at low temperatures, where the crystallization was extremely rapid, the Fisher–Turnbull equation was applied exclusively to crystallizations between 25 and 38°C. A plot of $\log(\tau T)$ vs. $1/T(\Delta T)^2$ also yielded two distinct linear regions of crystallization with a discontinuity occurring at 27ºC (Fig. 3). This suggested to us that the crystallization of either a second major fraction or a different polymorph was taking place below 27ºC. This discontinuity was also evident in a jump in the Avrami exponent (*n*) at a similar temperature (Fig. 2B). Characteristic double peaks in DSC melting profiles for palm oil reported in previous studies within this temperature regime lend further support to this suggestion (22,23). The slopes of each corresponding linear region in Figure 3 were then used to calculate the apparent free energies of nucleation for each distinct fraction.

Plots of the apparent activation free energies of nucleation

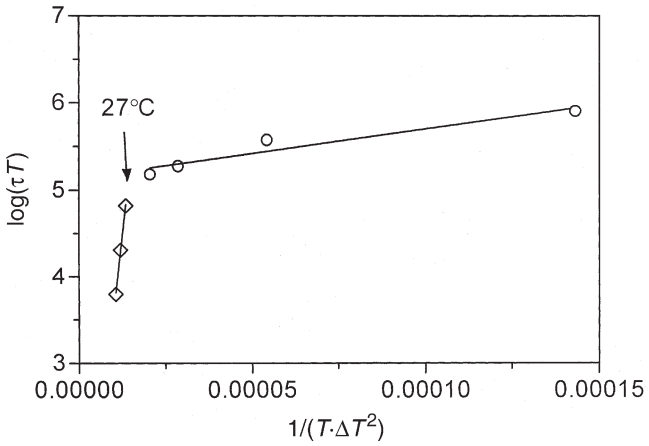

FIG. 3. The plot of $\log(\tau T)$ vs. $1/(T{\cdot}\Delta T^2)$ yields two distinct linear regions with slopes that permit the calculation of activation free energies of nucleation of each fraction according to $\Delta G_C = sk/(T_m - T)^2$, as has been indicated in the literature (13). Induction times of crystallization (τ, s) were determined by a cloud point analyzer.

as a function of temperature are shown in Figure 4. For each fraction, the free energy of nucleation was higher at higher temperatures (or lower degrees of supercooling), resulting in

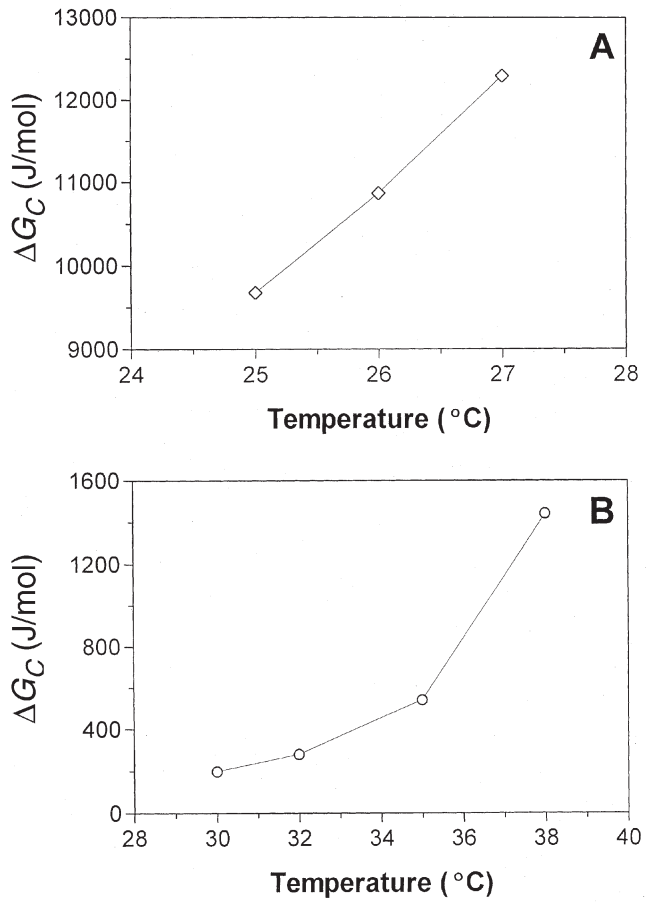

FIG. 4. (A) Activation free energies of crystallization (J/mol) vs. temperature (ºC) calculated from the slopes of the linear regions in Figure 3 for the fraction crystallizing in the range of 25 to 27ºC and (B) for the fraction crystallizing in the range of 30 to 38ºC.

lower nucleation rates at temperatures closer to the m.p. of the shortening. In addition to fractionation, the differences in crystallization behavior above and below the critical temperature of 27ºC may be due to differences in polymorphism. The less stable α polymorph may have formed at lower temperatures, whereas more stable β and/or β′ forms may have formed at higher temperatures. Similar findings have been reported in studies on the kinetics of nucleation in palm oil, trilaurin, and palm–sunflower oil mixtures (16,19,21). To investigate the effect of polymorphism and storage time on the properties of the shortening, we carried out DSC and XRD studies.

DSC. DSC experiments indicated that cooling rate strongly affected initial polymorphism (α vs. β′). Crystallizations were carried out at 23ºC with cooling from the melt carried out at different rates (Fig. 5A). Samples cooled at high rates (15ºC/min and 5ºC/min) showed single crystallization peaks, whereas those that were cooled slowly (1 and 0.5ºC/min) showed two peaks. Single peaks that occurred at higher cooling rates may have indicated the formation of the less stable α polymorph, without the occurrence of detectable fractionation, whereas double peaks that occurred at slower cooling conditions allowed for some fractionation and for crystallization to take place *via* the β′ polymorph (19). DSC melting curves obtained in the early stages of the crystallization process provided further support for this hypothesis (Fig. 5B). Samples crystallized at the two highest cooling rates displayed an exothermic recrystallization peak prior to the single endothermic melting peak, which remained the same for all samples. The occurrence of recrystallization peaks is likely due to a polymorphic transition from the α to the β′ upon melting of the unstable α form. Another set of samples was crystallized under the same conditions, but were stored isothermally for a period of 72 h before being subjected to the same melting treatment (Fig. 5C). No significant differences in the heat flow patterns were detected in the stored samples, suggesting that a transition of the fast-cooled samples from the α polymorph to the more stable β′ polymorph occurred during storage. As a result of this polymorphic transition during storage, recrystallization peaks were not observed. The same set of three experiments was also conducted isothermally at 5ºC, using the same cooling rates and storage conditions. Results of these experiments (not shown) were indicative of the same polymorphic behavior, with the α polymorph being formed by high cooling rates, apparent α to β′ transitions occurring at low cooling rates with recrystallization upon immediate melting, and β′ polymorphs occurring exclusively in stored samples. It is, however, necessary that differences in the number and shape of heat flow peaks obtained during crystallization and melting in DSC analysis not be interpreted exclusively as differences in polymorphism. The possibility does exist that the most stable but less favorable β polymorph may have occurred in addition to α and β′ polymorphs. The β′ form can be stable for years (depending on the TAG composition), and it is often desired during storage of fatty food products (15,17,18). The α polymorph, on the other hand, is very unstable and is normally only present during the processing and manufacture of fats, on a time scale of minutes or less (15). For this reason, powder XRD experiments examining the effects of degree of supercooling and storage time and temperature were also conducted.

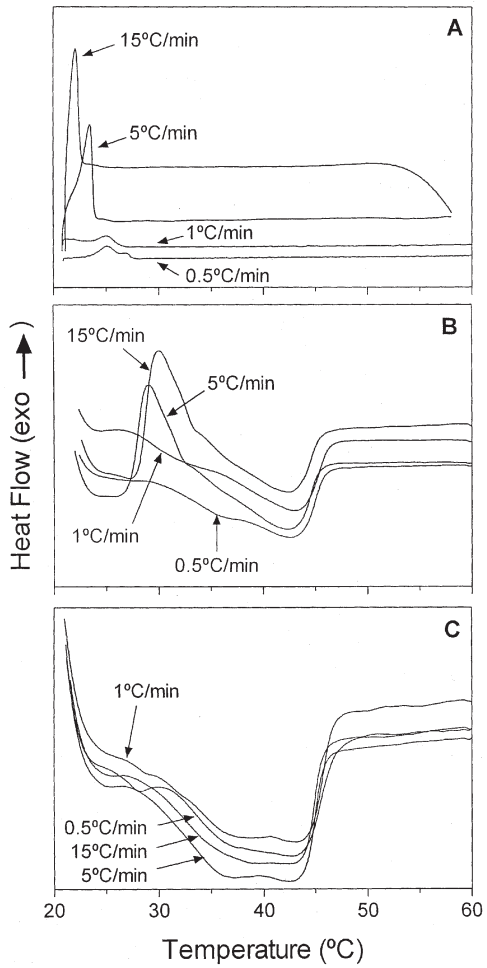

FIG. 5. (A) DSC crystallization curves for shortening samples taken from the melt (60ºC) to 23ºC at cooling rates of 15, 5, 1, and 0.5ºC/min. (B) Curves for the same newly crystallized samples immediately melted at a rate of 5ºC/min. (C) Curves for samples cooled at the four different rates after storage at 23ºC for 48 h.

Powder XRD spectroscopy. Powder XRD spectroscopy was performed on samples that were crystallized and stored at selected temperatures that represented differing degrees of supercooling and storage duration (Table 2). Results indicated that the β′ polymorph was dominant in all stored samples, independent of the degree of supercooling or cooling rate leading up to crystallization. To confirm the occurrence of the α polymorph early in the crystallization process at various degrees of supercooling, samples were taken from the melt, quenched to 28, 23, and 5ºC, and analyzed after a crystallization period of only 5 to 7 min. The samples in this case, as anticipated, took on the α polymorphic form, as was indicated by short spacings at either 4.17 or 4.28 Å. The sample that was cooled slowly in a stepwise manner to 5ºC and immediately analyzed also mirrored the results of the slowly cooled samples by DSC, having sufficient time to undergo the α to

TABLE 2
Powder XRD Spectroscopy Short-Spacings of Shortening Composed of Partially Hydrogenated Palm and Soybean Oils[a]

Temperature (°C)	Time of sample storage	Short-spacings (Å)	Polymorph
5	5 min	4.17(s)	α
5[b]	5 min	3.80(m), 4.20(s)	β′
23	7 min	4.28(w)	α
28	7 min	4.28(w)	α
5	6 d	3.80(m), 4.20(s)	β′
22	6 d	3.80(m), 4.20(s)	β′
26	6 d	3.80(m), 4.20(s)	β′

[a]s, strong; m, medium; w, weak. XRD, X-ray diffraction.
[b]Stepwise cooled (1 h storage at each step: 80ºC → 60ºC → 26ºC → 22ºC → 5 min at 5ºC).

β′ polymorphic transition before reaching the crystallization temperature.

Rheology. Table 3 shows the storage moduli (G'), loss moduli (G''), and tan δ (G''/G') values for the shortening crystallized in molds and held at 5, 22, and 27°C for 72 h. The storage and loss moduli of the network were independent of frequency in the linear viscoelastic region. Storage and loss moduli values decreased as temperatures increased from 5 to 27°C, indicating that crystallization temperature affected the mechanical response. Examining the changes in SFC relative to changes in G' provides further evidence that these two parameters do not display exact proportionality. Changing the crystallization temperature from 5 to 22ºC, and 22 to 27ºC, for example, results in a reduction in SFC of 46 and 22%, respectively. The actual measured G', however, changes in magnitude by 53 and 30% across these same temperatures, respectively, and may be due to changes in the parameters affecting crystal habit (polymorphism and/or microstructure).

The mechanical properties of a material, including the storage modulus (G'), are a function of the SFC, but other important factors that characterize crystal habit also have a significant influence. Polymorphism, and the parameters D_f and λ, which at the microstructural level characterize the spatial distribution of mass and the particle properties, respectively, also contribute to rheological properties.

Microscopy and image analysis. The microstructures of the shortening samples were visualized by PLM in order to investigate the effects of crystallization temperature on fat crystal network structure. Micrographs of samples crystallized and stored for 72 h at 27, 22, and 5ºC are shown in Figure 6. Discrete spherulitic crystals occurred in the samples crystallized at 27ºC (Fig. 6A). Crystallizations at 22ºC resulted in two different networks—one with smaller, more numerous crystals (Fig. 6B) and another that displayed a needle-like texture (Fig. 6C). At 5ºC (representing a high degree of supercooling), a granular texture was observed (Fig. 6D). Similar crystal morphologies were previously observed by Kawamura (16) during isothermal crystallization of palm oil and by Rousseau *et al*. (17,20) in crystallizations of nonesterified and interesterified palm oil and palm oil–soybean oil blends.

These differences in morphologies corresponded loosely to the trends found in the Avrami analysis (Fig. 2A). The Avrami exponent (n) is suggestive of more spherulitic growth at 27ºC (n = 3), disc-like growth at 22ºC (n = 2), and rod-like growth at 5ºC (n = 1) (13).

Also, at slow cooling rates the crystallization of separate fractions can be observed qualitatively in the form of two major crystal morphologies (Fig. 7A,B). Faster cooling rates, by contrast, result in more uniform crystal morphologies (Fig. 7C,D). These morphological characteristics may correspond to the presence of double and single crystallization peaks found by DSC. Mean particle diameters also decreased with faster cooling rates (Table 4).

The fractal dimensions (D_f) determined by the particle counting method are sensitive to the spatial distribution of the particles in the crystal network (7). Higher fractal dimensions occur in networks that are more ordered, whereas networks that arise from a more disordered nucleation and growth process result in lower fractal dimensions. The micrographs of the shortening in Figure 6 and their corresponding fractal dimensions (Table 4) demonstrate that the degree of supercooling does not drastically alter the spatial distribution of mass in the resulting crystal network. The fractal dimension remained relatively constant with decreases in the crystallization temperature from 27 to 5ºC. However, since all stored samples were in the β′ polymorph (Fig. 6), further experimentation is necessary to explore the effect of polymorphism on the fractal dimension.

TABLE 3
Network Microstructural and Rheological Characteristics of the Shortening as a Function of Crystallization Temperature[a]

Temperature (°C)	SFC (%)	G' (Pa) $\times 10^5$	G'' (Pa) $\times 10^4$	tan δ (G''/G')	D_f^{3d}	λ (MPa)
5	20.9	11.9 ± 0.9	6.8 ± 0.3	0.056	2.87 ± 0.06	2.05
22	11.4	5.0 ± 0.5	3.3 ± 0.8	0.075	2.92 ± 0.06	1.05
27	8.9	3.5 ± 0.6	2.6 ± 0.5	0.075	2.88 ± 0.06	0.82

[a]SD (n = 3) are indicated for the storage moduli G', loss modulus G'', and fractal dimensions (n = 10). SFC, solid fat content; D_f^{3d}, fractal dimension computed by image analyses translated into three dimensions.

TABLE 4
Fractal Dimensions (D_f), and Mean Particle Diameter Determined by Image Analysis of Shortening Samples Crystallized at Various Temperatures and Cooling Rates[a]

	Fractal dimension (D_f) (d = 2)	Mean particle diameter (μm)
Crystallization temperature (°C)		
5	1.87	1.0
22	1.92	1.7
27	1.88	1.2
Cooling rate (°C/min)		
1	1.98	1.6
1[a]	1.90	1.6
15	1.93	1.3
15[a]	1.92	1.4

[a]Samples imaged after 72 h storage at 22ºC.

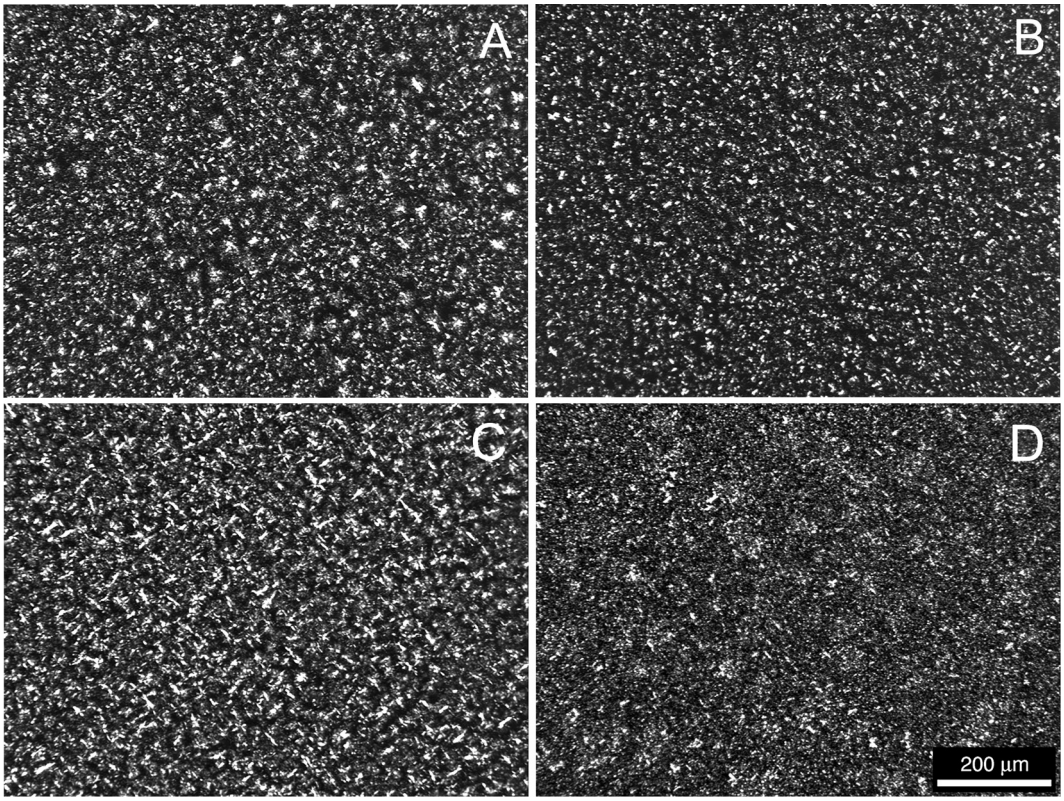

FIG. 6. Polarized light micrographs of shortening crystallized statically at (A) 27°C, (B and C) 22°C, and (D) 5°C, demonstrating the effects of degree of supercooling on morphology and spatial distribution of mass.

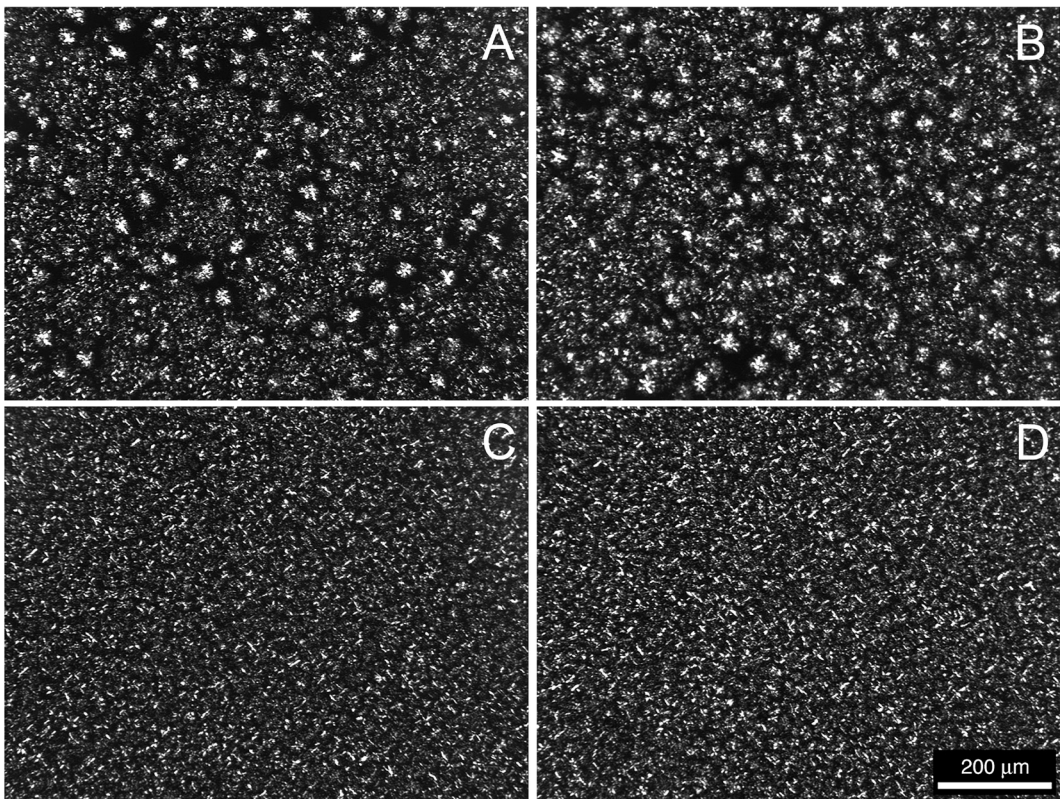

FIG. 7. Polarized light micrographs of shortening crystallized isothermally at 22°C under defined cooling rates and storage times: (A) 1°C/min imaged immediately, (B) 1°C/min imaged after 72 h storage, (C) 15°C/min imaged immediately, (D) 15°C/min imaged after 72 h of storage. Image analysis demonstrates the effects of degree of supercooling and polymorphism on morphology and spatial distribution of mass.

Therefore, crystallizations were conducted at 22ºC in an attempt to recreate and image the polymorphs found by DSC. Micrographs were acquired immediately after the crystallization temperature was reached by both fast and slow cooling rates, and after storage (Fig. 7). Cooling at 1ºC/min resulted in primarily spherulitic morphologies (Fig. 7A), whereas cooling at 15ºC/min resulted in smaller, more numerous needle-like crystals (Fig. 7C). These two different morphologies may be due in part to the presence of the β′ and α polymorphs, induced by the different cooling rates as shown by DSC (Fig. 5A). Micrographs of the same samples following 72 h storage at 22ºC, however, showed little change in both crystal morphology and particle diameter (Fig. 7B,D). The α to β′ transition that was observed by DSC (Fig. 5B,C) therefore does not result in a drastic change in crystal morphology.

Cooling rate had a small effect on the fractal dimensions obtained. At a slow cooling rate (1ºC/min), a D_f value of 1.98 was observed (Table 4), whereas the sample crystallized at the high cooling rate (15ºC/min) had a lower fractal dimension of 1.93. After storage for 72 h, micrographs of the samples cooled at 1 and 15ºC/min had fractal dimensions of 1.90 and 1.92, respectively. It is postulated that large changes in the spatial distribution of particles in the network upon storage are not likely to occur owing to the rigidity of the crystal network formed and the heightened viscosity of the remaining oil fraction. As well, for this system, cooling rate and the degree of supercooling did not affect the spatial distribution of mass.

Further efforts in modeling λ and the direct measurement of the particle properties that affect λ are an emphasis of the research being conducted in our laboratory. Advances in microscopy and image analysis will allow us to better observe and quantify parameters at the microstructural level that have effects on macroscopic rheological properties. Taking into account all factors that influence the physical properties of a fat will allow us to better design and control manufacturing processes and improve product quality.

ACKNOWLEDGMENTS

The authors acknowledge the financial assistance of the Natural Sciences and Engineering Research Council of Canada (NSERC), the Ontario Ministry of Agriculture, Food, and Rural Affairs (OMAFRA), the University of Buenos Aires, Consejo Nacional de Investigaciones Científicas y Técnicas de la República Argentina, and the Interamerican Development Bank.

REFERENCES

1. Yusem, G.J., and P.N. Pintauro, The Electrocatalytic Hydrogenation of Soybean Oil, *J. Am. Oil Chem. Soc. 69*:399–404 (1992).
2. DeMan, J.M., and A.M. Beers, Fat Crystal Networks: Structure and Rheological Properties, *J. Texture Studies 18*:303–318 (1987).
3. Heertje, I., Microstructural Studies in Fat Research, *Food Structure 12*:77–94 (1993).
4. Marangoni, A.G., and R.W. Hartel, Visualization and Structural Analysis of Fat Crystal Networks, *Food Technol. 52*:46–51 (1998).
5. Narine, S.S., and A.G. Marangoni, Fractal Nature of Fat Crystal Networks, *Phys. Rev. E 59*:1908–1920 (1999).
6. Narine, S.S., and A.G. Marangoni, Mechanical and Structural Model of Fractal Networks of Fat Crystals at Low Deformations, *Ibid. 60*:6991–7000 (1999).
7. Marangoni, A.G., Elasticity of High-Volume-Fraction Fractal Aggregate Networks: A Thermodynamic Approach, *Phys. Rev. B 62*:13951–13955 (2000).
8. Rousseau, D., K. Forestière, A.R. Hill, and A.G. Marangoni, Restructuring Butterfat Through Blending and Chemical Interesterification. 1. Melting Behavior and Triacylglycerol Modifications, *J. Am. Oil Chem. Soc. 73*:963–972 (1996).
9. Bannon, C.D., J.D. Craske, and A.E. Hilliker, Analysis of Fatty Acid Methyl Esters with High Accuracy and Reliability. IV. Fats with Fatty Acids Containing Four or More Carbon Atoms, *Ibid. 62*:1501–1507 (1985).
10. *Official Methods and Recommended Practices of the American Oil Chemists' Society*, 4th edn., AOCS Press, Champaign, 1993.
11. Marangoni, A.G., On the Use and Misuse of the Avrami Equation in Characterization of the Kinetics of Fat Crystallization, *Ibid. 75*:1465–1467 (1998).
12. Sharples, A., Overall Kinetics of Crystallization, in *Introduction to Polymer Crystallization*, edited by A. Sharples, Edward Arnold Ltd., London, 1966, pp. 44–59.
13. Wright, A.J., R.W. Hartel, S.S. Narine, and A.G. Marangoni, The Effect of Minor Components on Milk Fat Crystallization, *J. Am. Oil Chem. Soc. 77*:463–475 (2000).
14. Wang, T., E.G. Hammond, J.L. Cornette, and W.R. Fehr, Fractionation of Soybean Phospholipids by High-Performance Liquid Chromatography with an Evaporative Light-Scattering Detector, *J. Am. Oil Chem. Soc. 76*:1313–1321 (1999).
15. Kloek, W., Mechanical Properties of Fats in Relation to Their Crystallization, Ph.D. Thesis, Wageningen Agricultural University, Wageningen, The Netherlands, ISBN 90-5485-947-4, 1998.
16. Kawamura, K., The DSC Thermal Analysis of Crystallization Behavior in Palm Oil, *J. Am. Oil Chem. Soc. 56*:753–758 (1979).
17. Rousseau, D., A.G. Marangoni, and K.R. Jeffrey, The Influence of Chemical Interesterification on the Physicochemical Properties of Complex Fat Systems. 2. Morphology and Polymorphism, *Ibid. 75*:1833–1839 (1998).
18. Grall, D.S., and R.W. Hartel, Kinetics of Butterfat Crystallization, *Ibid. 69*:741–747 (1992).
19. Blaurock, A.E., Fundamental Understanding of the Crystallization of Oils and Fats, in *Physical Properties of Fats, Oils, and Emulsions*, edited by N. Widlak, AOCS Press, Champaign, 1999, pp. 1–32.
20. Marangoni, A.G., and D. Rousseau, The Influence of Chemical Interesterification on the Physicochemical Properties of Complex Fat Systems. 3. Rheology and Fractality of the Crystal Network, *J. Am. Oil Chem. Soc. 75*:1633–1636 (1998).
21. Kloek, W., P. Walstra, and T. van Vliet, Crystallization Kinetics of Fully Hydrogenated Palm Oil in Sunflower Oil Mixtures, *Ibid. 77*:389–398 (2000).
22. Siew, W.L., and W.L. Ng, Partition Coefficient of Diglycerides in Crystallization of Palm Oil, *Ibid. 72*:591–595 (1995).
23. Che Man, Y.B., T. Haryati, H.M. Ghazali, and B.A. Asbi, Composition and Thermal Profile of Crude Palm Oil and Its Products, *Ibid. 76*:237–242 (1999).

[Received September 25, 2001; accepted April 2, 2002]